CHAPTER 8

Results and Discussion (Part V):
In-Mg Codoped ZnO Films

Deposition and properties of the effects of In and Mg doping on ZnO films are investigated in this chapter. These films were deposited by the ultrasonic spray pyrolysis technique and the properties such as thickness, crystal structure, morphology, optical properties and electrical properties were measured.

8.1 Film preparation

8.1.1 Starting solution preparation

The starting solutions for In-Mg codoped ZnO films were prepared from $Zn(CH_3OO)_2 \cdot 2H_2O$ with $(CH_3COO)_2Mg \cdot 4H_2O$ and $InCl_3$ as dopants, which were dissolved in ethanol (C_2H_5OH) and deionized water (DI water) in the volume ratio of 1:3. Hydrochloric (HCl) acid was added to increase the solubility. The compositions of these solutions were a fixed 0.02 M of $Zn(CH_3OO)_2.2H_2O$ and 20 at.% Mg while the atomic percentage ratio of In/Zn was varied from 0 to 8 at.%, as listed in Table 8.1.

8.1.2 Spray coating

All starting solutions were sprayed on microscope glass substrates heated at 400°C by using ultrasonic spray pyrolysis in air. The distance between the nozzle and the substrate was 20 cm with nozzle frequency of 34 kHz and spray rate of 2.5 ml/min for a total time of 3 min. The schematic diagram of the In-Mg doped ZnO film fabrication process of this chapter was similar fabrication process of previous chapter 6 and is shown in Figure 6.1.

Table 8.1 Specifications materials and compositions of the starting solutions of In-Mg codoped ZnO films used in this study.

Materials	Source	Purity	Solution compositions
$Zn(CH_3OO)_2 \cdot 2H_2O$	Sigma-Aldrich	≥98%	0.02 M
$(CH_3COO)_2Mg \cdot 4H_2O$	Sigma-Aldrich	≥99%	20 at.% Mg
$InCl_3$	Sigma-Aldrich	99.999%	0-8 at% In
C_2H_5OH	EMSURE®	absolute	25 % of solution
DI water	-	-	75 % of solution
HCl	EMSURE®	37%	0.01 M

8.2   Results and discussions

Images of In-Mg codoped ZnO films with different In concentrations deposited on glass substrates are shown in Table 8.1. It was found that all films had high transparency. The characterizations of these films such as thickness, crystal structure, morphology optical and electrical properties are described in the following sections.
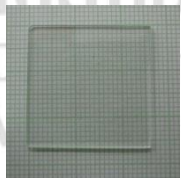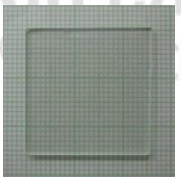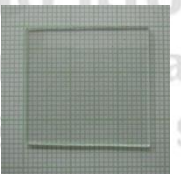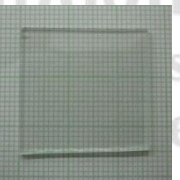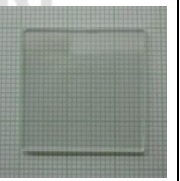
Substrate temp. (°C)	In doping				
	0 at.%	2 at.%	4 at.%	6 at.%	8 at.%
400					

Figure 8.1 The appearance of In-Mg codoped ZnO films with different In concentrations.

8.2.1 Thickness

Figure 8.2 showed the SEM cross section microstructures of In-Mg codoped ZnO films with different In concentrations on glass substrate, which were investigated by SEM technique. It was observed that the films grew well on the glass substrates. The thicknesses of films were estimated from these images and are listed in Table 8.2. All films showed almost same thickness, which were in the range 200-230 nm. The thicknesses of films depend on the time of spraying and flow rate of solution. The thickness of the films with different In concentrations was in the same order.
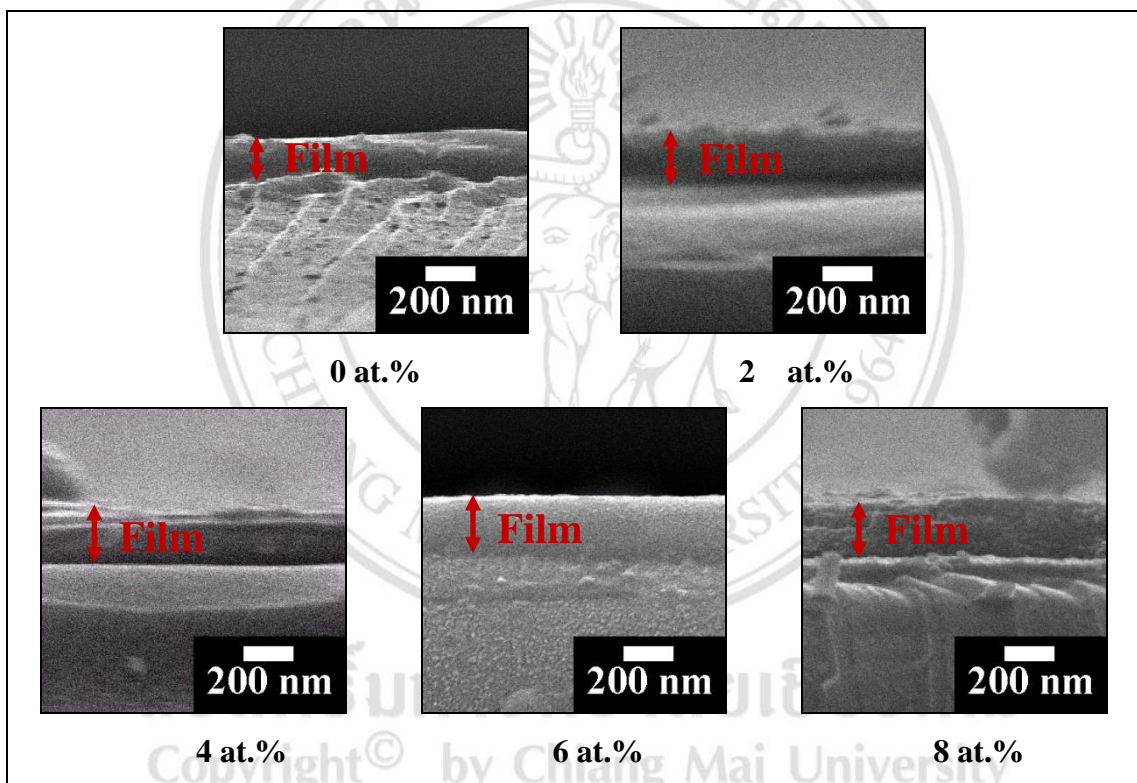

Figure 8.2 The cross section microstructures of In-Mg codoped ZnO films with different In concentrations.

Table 8.2 Thickness of In-Mg codoped ZnO films different In concentrations.

In concentration (at.%)	Thickness (nm)	
	Value	SD
0	203.2	14.0
2	221.5	7.3
4	227.8	9.8
6	230.2	4.7
8	217.6	14.2

8.2.2 Crystal structure

The XRD patterns of In-Mg codoped ZnO films with different In concentrations are shown in Fig. 8.3. All films were identified as polycrystalline hexagonal wurtize ZnO structure with preferred orientation along the (002) plane. The height of this plane increased with addition In concentration to 4 at.% and decreased with future addition of Mg concentration. This result was also observed in In doped ZnO films in other research [62,65,93]. This behavior was in consistent with the increasing of (400) plane of ITO film, which was reported in chapter 4. The increasing of crystalline phase was occurred due to the impurities doping was substituted into the primary atom sites caused to the increasing of crystalline phase of films [77]. However, Further increased of impurity doping was over solubility limit into lattice, the crystallinity reduces may be due to excessive impurities, which may form into secondary phase [78].

In addition, the XRD analysis showed the $Ca_2Al_{1.5}Fe_{0.5}SiO_7$. It could be expected that this phase was crystal phase of the glass substrate, which was explained in chapter 6.
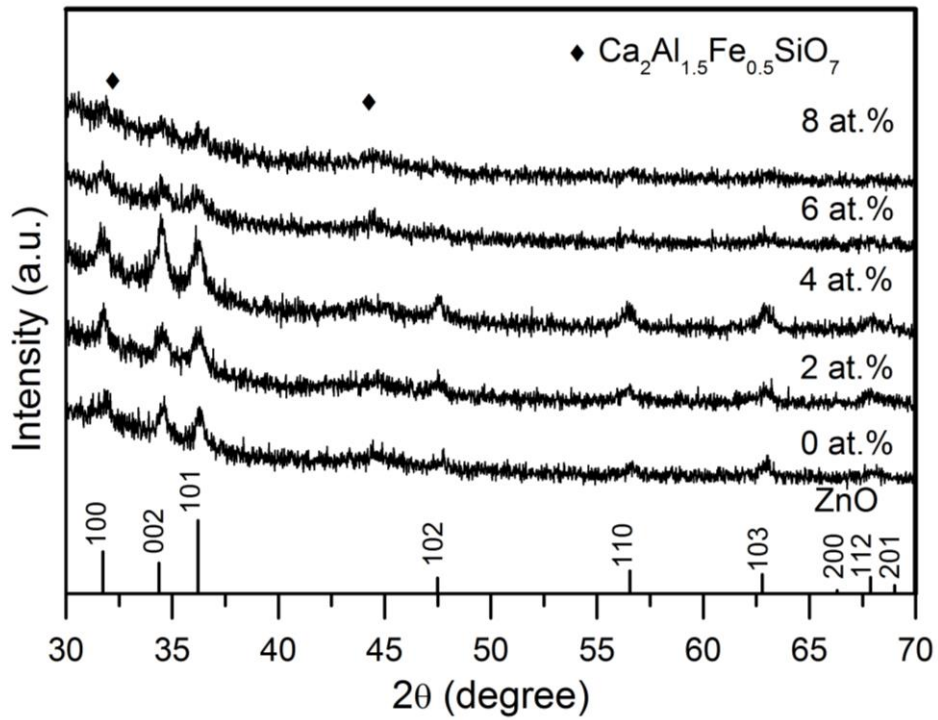
110

Figure 8.3 The XRD patterns of In-Mg codoped ZnO films with different In concentrations.

Table 8.3 Crystallite size of (002) and (101) planes of In-Mg codoped ZnO with different In concentrations.

In concentrations (at.%)	Crystallite size (nm)	
	hkl (002)	hkl (101)
0	25.35	30.49
5	25.55	21.81
10	26.47	22.06
15	28.14	20.54
20	25.65	19.15

The crystallite sizes of In-Mg codoped ZnO films with different In concentrations are listed in Table 8.3. The crystallite sizes of these films can be calculated from FWHM values of (002) and (101) peaks by equation 3.2.

111

The crystallite size of the (002) peaks were almost the same. While, the crystallite size variation of the (101) peak decreased with increasing In concentrations.

8.2.3 Morphology

Surface morphology of In-Mg codoped ZnO films with different In concentrations deposited on the glass substrates were investigated by SEM and AFM techniques and shown in Figure 8.4 and 8.5, respectively. The average grain size and surface roughness of films were obtained from these SEM and AFM images, respectively were presented in Figure 8.6.
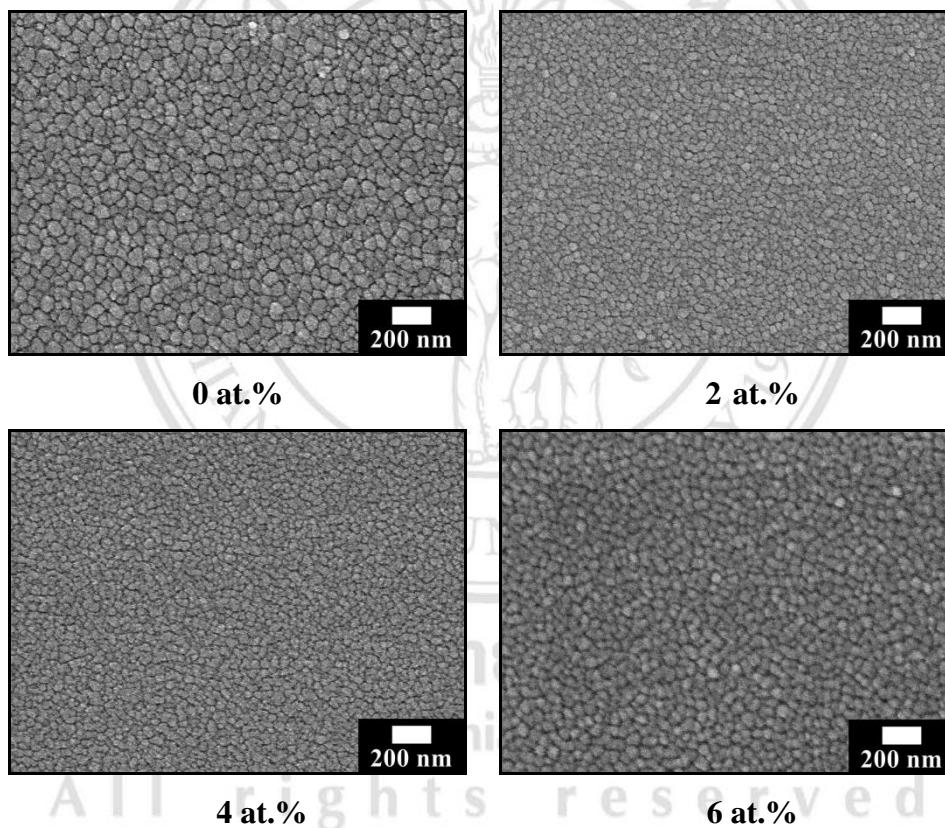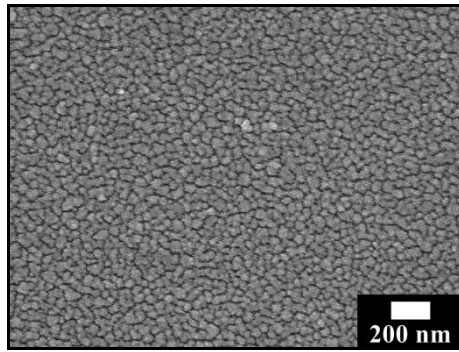

Figure 8.4 SEM images of Mg doped ZnO films with different In concentrations.

8 at.%

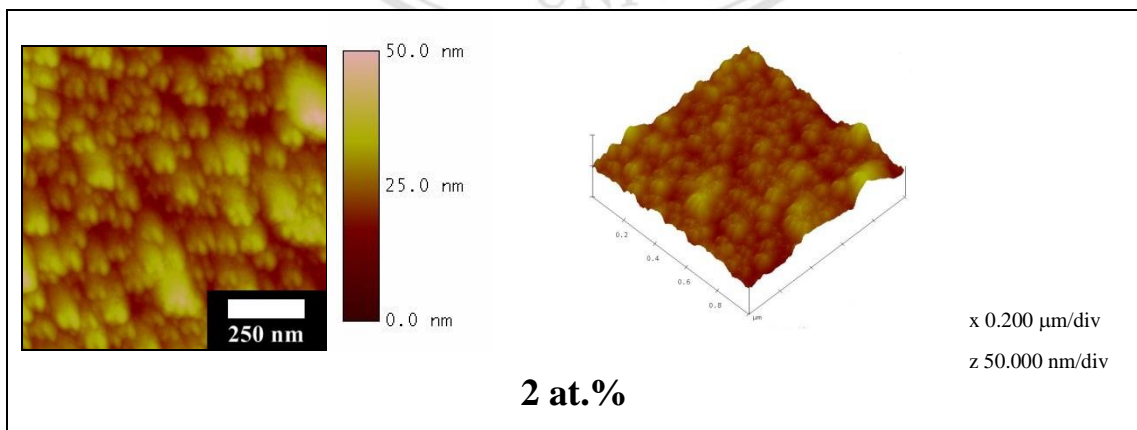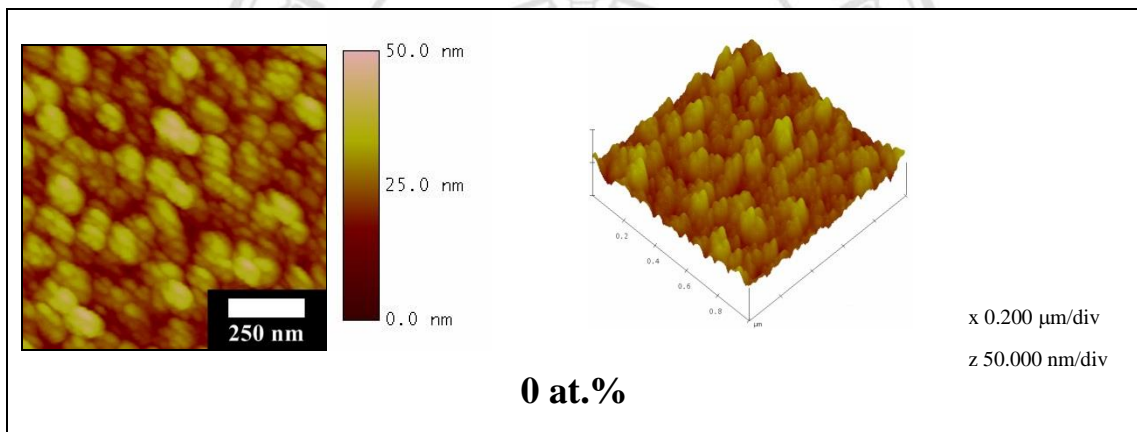Figure 8.4 SEM images of Mg doped ZnO films with different In concentrations (continued).

0 at.%

2 at.%

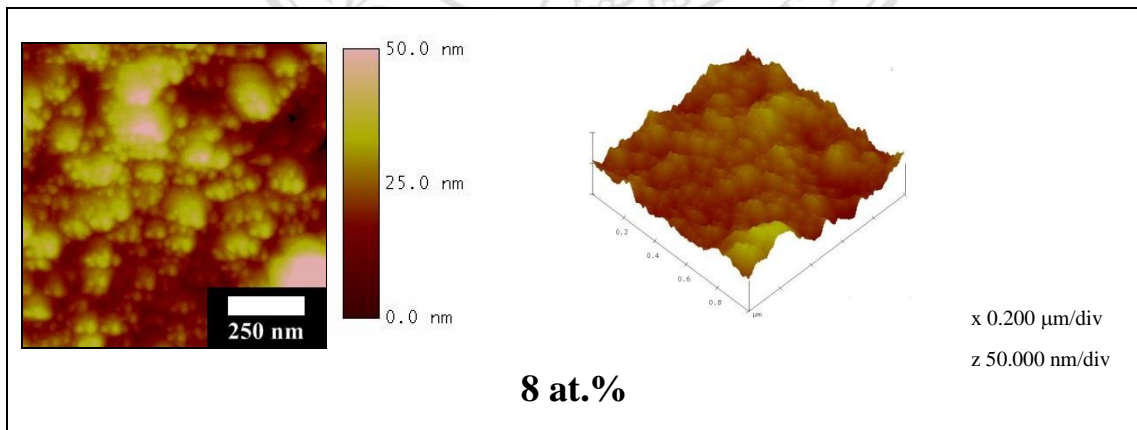Figure 8.5 AFM images of In-Mg codoped ZnO with different In concentrations.
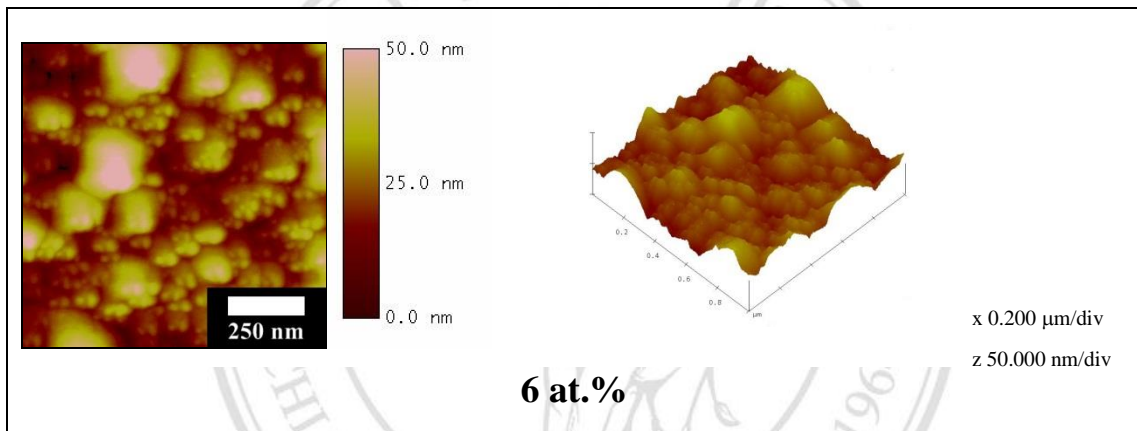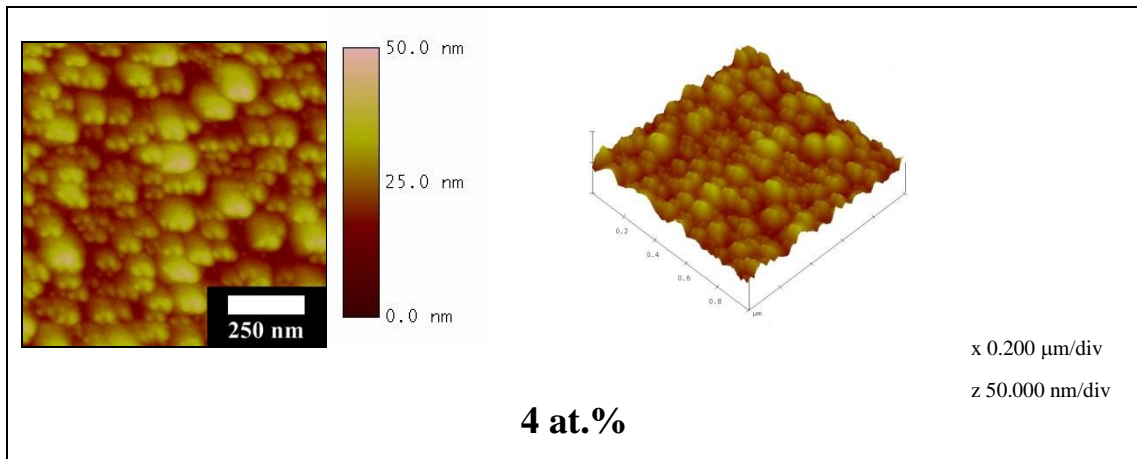
Figure 8.5 AFM images of In-Mg codoped ZnO with different In concentrations

(continued).

From SEM and AFM images, it was found that all films are homogeneous films with spherical shape and low surface roughness. It was also found that the average grain size of In-Mg codoped ZnO films showed lower than Mg doped ZnO film, which was similar to the results of In doped ZnO film [94].

114

The surface roughness of In-Mg codoped ZnO films with addition of In at 2 at.% showed lower than the Mg doped ZnO film and increased with increased In concentration more than 2 at.%.
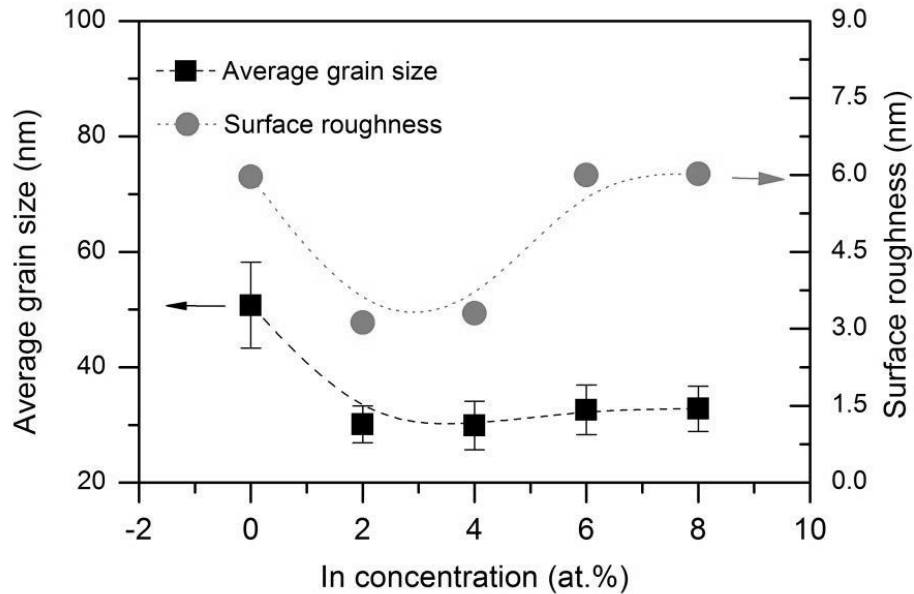

Figure 8.6 Average grain size and surface roughness of In-Mg doped ZnO films with different In concentrations.

8.2.4 Optical properties

The transmittance and absorbance spectra over the wavelength range 300-1000 nm of glass substrate and In-Mg codoped ZnO films with different Mg concentration are shown in Figure 8.7. It was found that all films presented a sharp ultraviolet cutoff. The transmittance of In-Mg codoped ZnO films were found to decrease with increasing In concentration and the absorption edge of In-Mg codoped ZnO films shifted to higher wavelengths (redshift) with addition of In.

The band gap was evaluated from this transmittance spectra and thickness (Table 8.2) using Tuac's relationship in equation 3.8. The $(\alpha h \nu)^2$ versus $h\nu$ plots of all films are shown in Figure 8.8 (a) The intercept of $(\alpha h \nu)^2$ on the x-axis gave the value of the direct band gap and the band gap of all films showed in Figure 8.8 (b). It was found that, the band gap values decreased

115

with increasing In concentration. *Jung et al* [66] explained the decreasing of the band gap as an effect of the merging of a donor level and the conduction band at high impurity density. Thus, redshift occurs due to increasing carrier density. However, the band gap of codoped ZnO films with 2-4 at.% In are in a suitable range for optoelectronic applications.
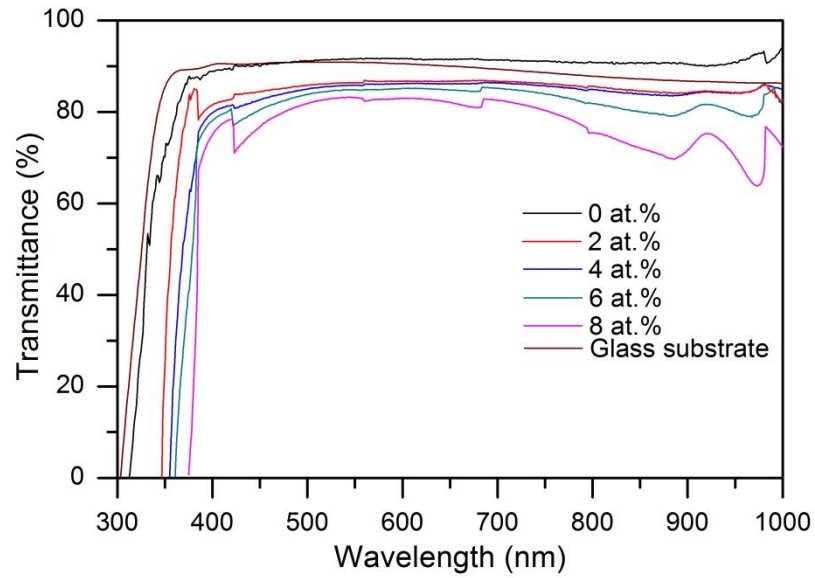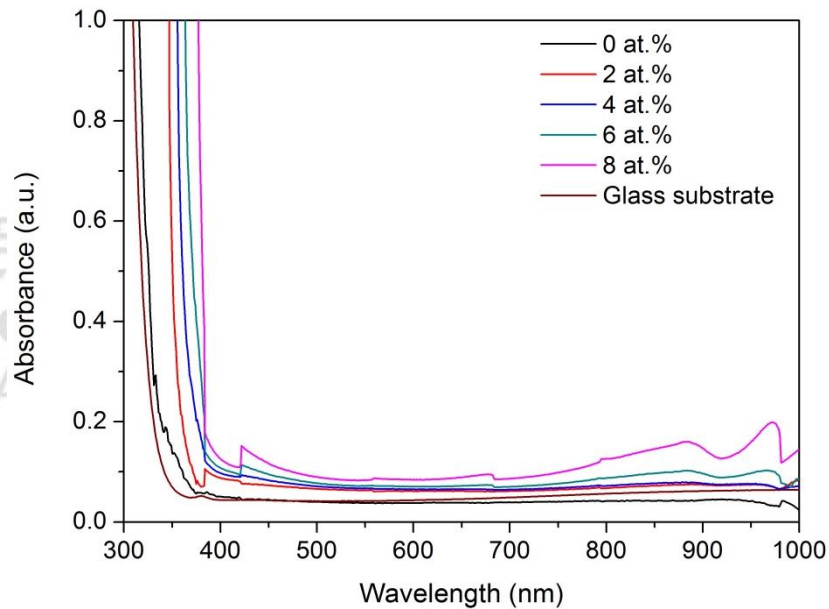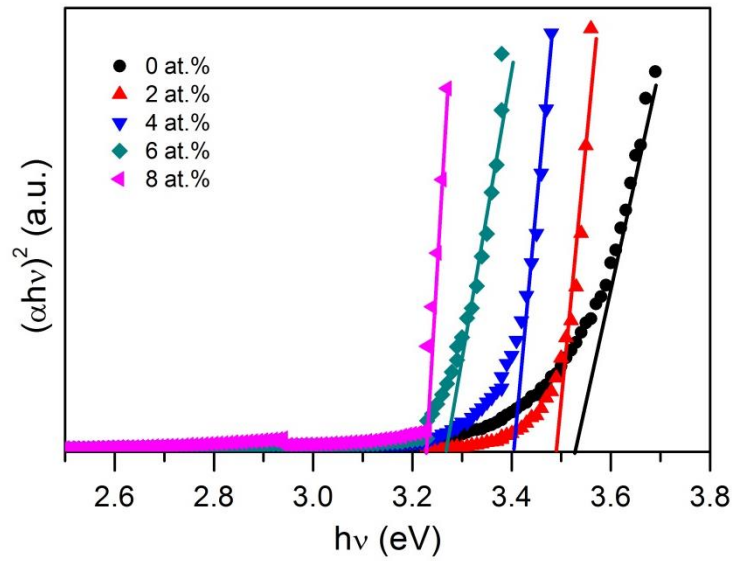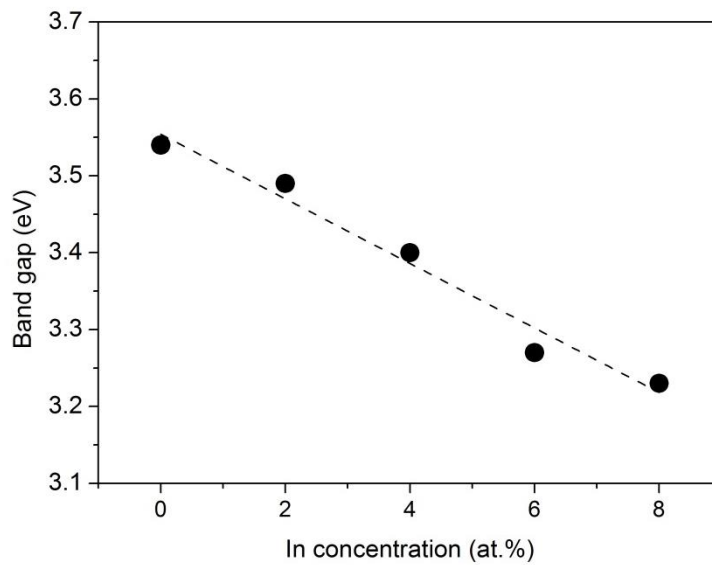

(a) Transmittance

Figure 8.7 Transmittance (a) and absorbance (b) spectra of In-Mg cpodoped ZnO films with different In concentrations.

116

(a) $(\alpha h\nu)^2$ **versus** $h\nu$ **plots**

(b) Band gap

Figure 8.8 The $(\alpha h\nu)^2$ versus $h\nu$ plots of In-Mg codoped ZnO with different Mg
concentrations (a) and band gap (b) of these films.

8.2.5 Electrical property

The sheet resistance and the resistivity of In-Mg codoped ZnO films with
different In concentrations are shown in Figure 8.9. The resistivity is

calculated from resistance and thickness of films by equation 3.10, the thickness was listed in Table 8.2. The resistivity of In-Mg codoped ZnO films decreased with increasing In concentration until 4 at.% and increased for higher In concentration more than 4 at.%. For comparison, the resistivity of indium doped ZnO films has been reported to decrease and showed lowest resistivity for the range 2-3 at.% of In concentration [62,93], the result of this work is in accordance to their work. The resistivity behavior can be described as the electrical conductivity of In doped ZnO films as due to the electron, which was generated by ionization of the interstitial zinc atom and oxygen vacancies [62,93]. The In^{3+} atom can substitute for Zn^{2+} atom or can take interstitial positions in the ZnO lattice so this In^{3+} atom act as donor [62], which leads to decrease of resistivity of films with addition of In. However, there is a limitation of In concentration solubility in ZnO lattice, observed from the resistivity of films increased with doping of In more than 4 at.%. Then, the remainder of In can result in impurity segregation and collected at the grain boundary [62].
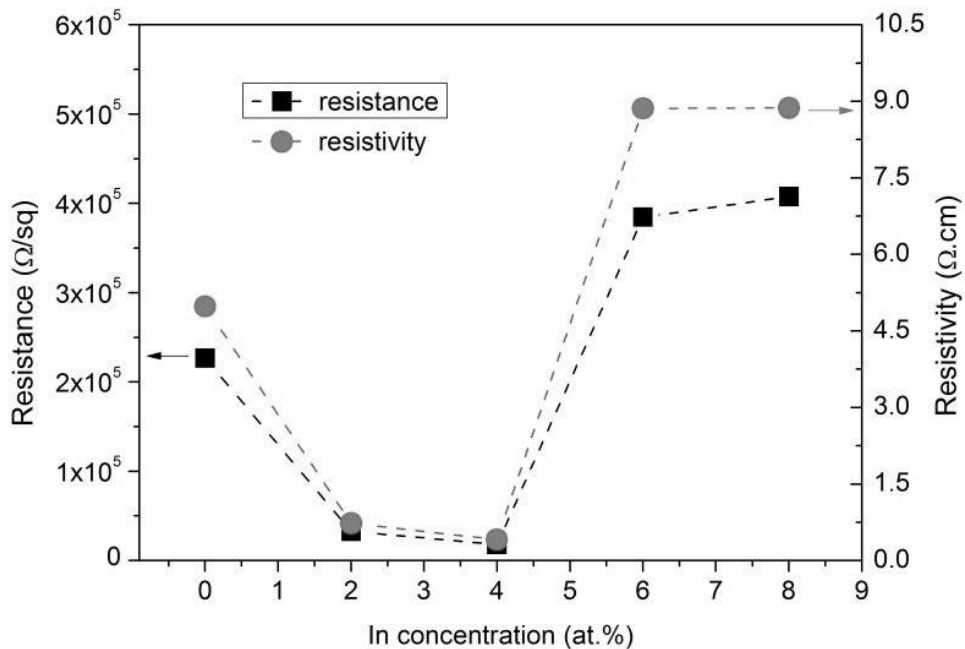

Figure 8.9 The sheet resistance and the resistivity of of In-Mg codoped ZnO with different In concentration.